Combined Autonomous Absolute and Relative Orbit Control in Low Earth Orbit

Sergio De Florio[(1)], **Simone D'Amico**[(2)], **and Gianmarco Radice**[(1)]
[(1)]*Space Advanced Research Team, School of Engineering, University of Glasgow, Glasgow G12 8QQ, UK, s.de-florio.1@research.gla.ac.uk*
[(2)]*DLR, Space Flight Technology Department, D-82230 Wessling, Germany*

Abstract: *The recent advances in the field of autonomous absolute and relative orbit control render this technology mature to be used on a routine basis. The step forward in this research is the study of the possibility of combining autonomous absolute and relative orbit control. This paper analyses the problem of the combined autonomous absolute and relative control of a two spacecraft formation in low Earth orbit. One of the two spacecraft keeps its mean orbital elements within their control window whereas the other spacecraft controls the relative motion. The autonomous formation control is meant to meet the distributed payload requirements and to keep the formation safe from a collision risk. The collision avoidance criterion used is the maintenance of a (anti-)parallel alignment of the relative eccentricity and inclination vectors. The overall strategy is verified, by means of numerical simulations, using the TerraSAR-X/TanDEM-X formation as simulation scenario. The simulation results are evaluated and compared with the actual values acquired during the routine operations of the TSX/TDX formation. A first conclusion can thus be formulated about the advantages and disadvantages in the exploitation of an autonomous on-board orbit control with respect to a ground based system.*

Keywords: *Autonomous, orbit, control, formation.*

1. Introduction

Nowadays the experience in ground-in-the-loop absolute and relative orbit control with strict requirements [1,2] is consolidated. The employment of an autonomous on-board orbit control system poses the problem of evaluating in which terms it could be more convenient than a ground-based orbit control. An on-board control system can fulfil very strict control requirements on different orbit parameters in real-time and with a significant reduction of flight dynamics ground operations. On the other end, it can interfere with the payload operations planning and can be more delta-v demanding than a ground-in-the-loop orbit control system. The recent theory advances and the in-flight experience of autonomous absolute [3-5] and relative [6-9] orbit control are paving the way for the routine use of this technology in the near future. The step forward in this research is the study of the possibility of combining autonomous absolute and relative orbit control. This paper analyses the problem of the combined autonomous absolute and relative control of a two spacecraft formation in Low Earth Orbit (LEO) using different types of on-board feedback control. One of the two spacecraft keeps its orbit's parameters within the control windows imposed around nominal values which characterize a reference orbit. The other spacecraft controls instead the relative motion. A distributed control tasks assignment over time is suggested in order to keep the mass of the two spacecraft as similar as possible. With this approach the differential drag, and thus the fuel consumption, can be minimized and the mission lifetime maximized. The autonomous formation control is meant to meet the

payload requirements and to keep the required formation geometry safe from a collision risk. The collision avoidance criterion used is the maintenance of a (anti-)parallel alignment of the relative eccentricity and inclination vectors [7]. In this context the autonomous control has an added value as it allows a prompt reaction to unexpected events. The secular non-keplerian perturbation forces acting on both satellites alter the nominal formation configuration. The most critical change is the clockwise drift of the relative eccentricity vector δe that tends to the perpendicular of the relative inclination vector δi, thus increasing the collision risk. As a consequence, the formation must be controlled to maintain the predefined orientation of the two vectors. A ground-based control has to regularly keep the formation configuration by commanding small orbit correction maneuvers. In most cases the ground station contacts are limited due to the geographic position of the station and the costs for contact time. A ground station placed at a middle latitude allows about two scheduled contacts every twelve hours for a LEO satellite. Only the availability of a polar ground station guarantees a contact at each orbit. While this limitation is usually not critical for single satellite operations, the visibility constraints determine the achievable orbit control accuracy for a LEO formation if a ground based approach is chosen. An autonomous relative orbit control system can provide a robust formation keeping improving the control performance as the orbital maneuvers are planned and executed more frequently. The combination of autonomous absolute and relative orbit control can thus enhance the overall control performance, reactivity in case of contingency and reduce the ground support efforts and costs.
Analytical and numerical control methods have been considered. The overall strategy is verified using the TerraSAR-X/TanDEM-X (TSX/TDX) formation [2,10] as simulation scenario. The formation TSX/TDX is realized in a public-private partnership between the German Aerospace Center and Astrium GmbH, and was built in 2010 with the launch of the satellite TanDEM-X. The primary objective is the generation of a global digital elevation model (DEM) with unprecedented accuracy by means of high-resolution Synthetic Aperture Radar data. This is the typical LEO remote sensing mission which could take advantage of the autonomous orbit control discussed here. The simulation results are evaluated from a performance, cost and operational point of view and compared with the actual values acquired during the routine operations of the TSX/TDX formation. A first conclusion can thus be formulated about the advantages and drawbacks in the exploitation of an autonomous on-board orbit control system.

2. Collision Risk Assessment for Co-orbiting Spacecraft

2.1. Computation of Closest Approach

The concept of e/i-vector separation has originally been developed for the safe collocation of geostationary satellites [11], but can likewise be applied for proximity operations in LEO formations and has been already implemented in the formation missions GRACE [12], TSX/TDX and PRISMA [13]. It is based on the consideration that the uncertainty in predicting the along-track separation of two spacecraft is generally much higher than for the radial and cross-track component. Because of the coupling between semi-major axis and orbital period, small uncertainties in the initial position and velocity result in a

corresponding drift error and thus a secularly growing along-track error. Predictions of the relative motion over extended periods of time are therefore particularly sensitive to both orbit determination errors and maneuver execution errors. To avoid a collision hazard in the presence of along-track position uncertainties, care must be taken to properly separate the two spacecraft in radial and cross track direction.
Using the relative orbital elements (ROE) parametrization ($\delta a, \delta e_x, \delta e_y, \delta i_x, \delta i_y, \delta u$), this can be achieved by imposing a parallel (or anti parallel) alignment of the relative eccentricity $\boldsymbol{\delta e} = (\delta e_x \delta e_y)^T$ and inclination $\boldsymbol{\delta i} = (\delta i_x \delta i_y)^T$ vectors. A collision risk assessment can be therefore defined by the evaluation of the minimum separation between the spacecraft in the $\mathbf{RTN}$ orbital frame ($\mathbf{R}$ pointing along the orbit's radius, $\mathbf{N}$ pointing along the angular momentum vector and $\mathbf{T} = \mathbf{N} \times \mathbf{R}$ pointing in the direction of motion for a circular orbit). The separation between the spacecraft in the NR plane is expressed by

$$\frac{\delta r_{RN}}{a} = \frac{1}{a}\sqrt{\delta r_R^2 + \delta r_N^2} \tag{1}$$

The problem of minimizing $(\delta r_{RN}/a)^2$ can be easily solved by substituting in Eq. (1) $\delta r_R/a = \delta a - \cos u \ \delta e_x - \sin u \ \delta e_y$, $\delta r_N = \sin u \ \delta i_x - \cos u \ \delta i_y$ [6] and operating the following change of variables

$$\frac{\delta R_R}{a} = \frac{\delta r_R}{a} - \delta a \quad , \quad \frac{\delta R_N}{a} = \frac{\delta r_N}{a} \tag{2}$$

as in this case the problem is reduced to finding the minimum of $(\delta R_{RN}/a)^2 = \mathbf{u}^T \mathbf{A} \mathbf{u}$ which is the quadratic form given by

$$\left(\frac{\delta R_R}{a}\right)^2 + \left(\frac{\delta R_N}{a}\right)^2 = \begin{pmatrix}\cos u \\ \sin u\end{pmatrix}^T \begin{pmatrix}\delta e_x^2 + \delta i_y^2 & \delta e_x \delta e_y - \delta i_x \delta i_y \\ \delta e_x \delta e_y - \delta i_x \delta i_y & \delta e_y^2 + \delta i_x^2\end{pmatrix} \begin{pmatrix}\cos u \\ \sin u\end{pmatrix} \tag{3}$$

The quadratic form $(\delta R_{RN}/a)^2$ admits a finite minimum only if it is positive definite. A quadratic form is positive definite if all the north-west principal minors of matrix A in Eq. (3) have a strictly positive determinant. This condition translates into

$$\delta e_x^2 + \delta i_y^2 > 0 \quad , \quad \begin{vmatrix}\delta e_x^2 + \delta i_y^2 & \delta e_x \delta e_y - \delta i_x \delta i_y \\ \delta e_x \delta e_y - \delta i_x \delta i_y & \delta e_y^2 + \delta i_x^2\end{vmatrix} > 0 \tag{4}$$

The first term of Eq. (4) is true $\forall \delta e_x, \delta i_y$, whereas the second term can be written as

$$(\boldsymbol{\delta e} \cdot \boldsymbol{\delta i})^2 > 0 \equiv \boldsymbol{\delta e} \ \text{ not} \perp \ \boldsymbol{\delta i} \tag{5}$$

Eq. (5) states that in case of bounded relative motion (i.e., $\delta a = 0$) and no uncertainties on the estimation and control of the relative orbital elements, a separation in the NR plane can be granted only if $\boldsymbol{\delta e}$ is not perpendicular to $\boldsymbol{\delta i}$. Vice-versa perpendicular relative e/i-vectors provide an unsafe configuration where radial and cross-track vanish at the same time as shown in Fig. 1. In order to find the minimal value of $(\delta R_{RN}/a)^2 = q(\mathbf{u}) = \mathbf{u}^T \mathbf{A} \mathbf{u}$

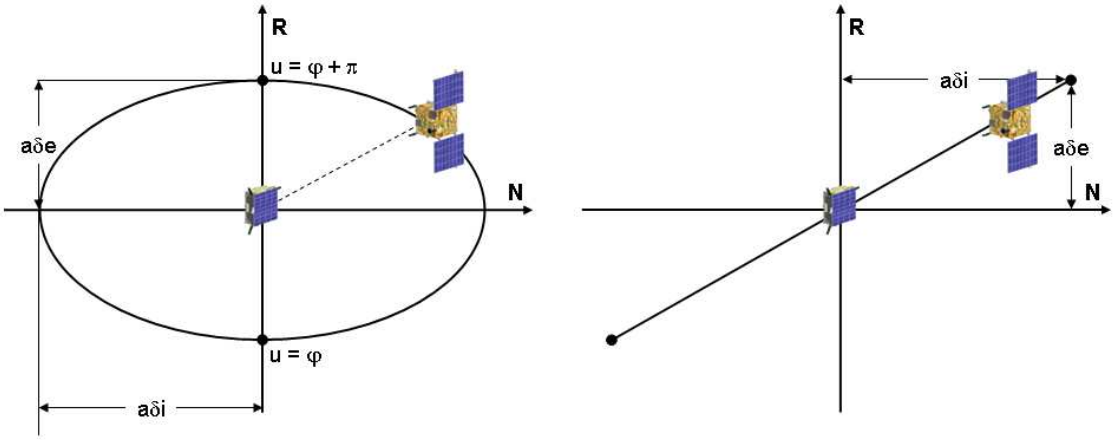

Figure 1. Projection of relative motion in the cross-track/radial plane for parallel (left) and orthogonal (right) relative e/i-vectors [6]

the following positive definite quadratic forms' property can be exploited

$$q(\mathbf{u}) \geq s_{min}\|\mathbf{u}\|^2 \tag{6}$$

where $\|\mathbf{u}\|^2$ as $u = (\cos u \sin u)^T$ and s_{min} is the minimum eigenvalue of matrix $\mathbf{A}$ in Eq. (3)

$$s_{min} = \frac{\delta e^2 + \delta i^2 - \sqrt{(\delta e^2 + \delta i^2)^2 - 4(\boldsymbol{\delta e} \cdot \boldsymbol{\delta i})^2}}{2} \tag{7}$$

Using the binomial factorization in Eq. (7)

$$\begin{aligned} s_{min} &= \frac{\delta e^2 + \delta i^2 - \sqrt{(\delta e^2 + \delta i^2 + 2\boldsymbol{\delta e} \cdot \boldsymbol{\delta i})(\delta e^2 + \delta i^2 - 2\boldsymbol{\delta e} \cdot \boldsymbol{\delta i})}}{2} = \\ &= \frac{\delta e^2 + \delta i^2 - \|\boldsymbol{\delta e} + \boldsymbol{\delta i}\| \cdot \|\boldsymbol{\delta e} - \boldsymbol{\delta i}\|}{2} = \frac{\left(\|\boldsymbol{\delta e} + \boldsymbol{\delta i}\| - \|\boldsymbol{\delta e} - \boldsymbol{\delta i}\|\right)^2}{4} \end{aligned} \tag{8}$$

$(\delta R_{RN}/a)_{min} = s_{min}$ can thus be written in vectorial notation as

$$\left(\frac{\delta R_{RN}}{a}\right)_{min} = \frac{\left(\|\boldsymbol{\delta e} + \boldsymbol{\delta i}\| - \|\boldsymbol{\delta e} - \boldsymbol{\delta i}\|\right)}{2} \tag{9}$$

It is noteworthy that the problem of minimizing $(\delta r_{RN}/a)^2$ can also be solved as the optimization problem of a two variables function $f(x, y)$ subject to the equality constraint $g(x, y) = 0$ (with $x = \cos u$ and $y = \sin u$)

$$f(x,y) = \delta e_x x^2 + \delta e_y y^2 + 2\delta e_x \delta e_y xy + \delta i_x x^2 + \delta i_y y^2 - 2\delta i_x \delta i_y xy \quad , \quad g(x,y) = x^2 + y^2 - 1 \tag{10}$$

Changing back to variables $\delta r_R/a$ and $\delta r_N/a$, as it has to be $\delta R_{RN}/a \geq (\delta R_{RN}/a)_{min}$, it

results

$$\left(\frac{\delta R_{RN}}{a}\right)^2 = \left(\frac{\delta R_R}{a} - \delta a\right)^2 + \left(\frac{\delta R_N}{a}\right)^2 \geq \left(\frac{\delta R_{RN}}{a}\right)^2_{min} \tag{11}$$

and considering that $\delta r_{RN}/a$ is given by Eq. (1), the inequality shown in Eq. (11) can be written as

$$\left(\frac{\delta r_{RN}}{a}\right)^2 \geq \left(\frac{\delta R_{RN}}{a}\right)^2_{min} + \delta a^2 - 2\delta a \delta e \cos(u - \varphi) \tag{12}$$

As $(\delta R_{RN}/a)_{min}$ and δa are not dependent on u and $(\delta R_{RN}/a)^2_{min}$ and δ^2 are always positive quantities, the second member of inequality in Eq. (12) has its minimum value when $\delta a \delta e \cos(u - \varphi)$ has its maximum positive value. Then the following inequality is always true

$$\frac{\delta r_{RN}}{a} \geq \sqrt{\left(\frac{(\|\boldsymbol{\delta e} + \boldsymbol{\delta i}\| - \|\boldsymbol{\delta e} - \boldsymbol{\delta i}\|)}{2}\right)^2 + \delta a^2 - 2\delta a \delta e} \tag{13}$$

The second member of Eq. (13) represents a minimal upper bound of $\delta r_{RN}/a$ and coincides with the minimum $(\delta r_{RN}/a)_{min}$ only in case $\boldsymbol{\delta e}$ and $\boldsymbol{\delta i}$ are parallel.

2.2. Collision Risk Assessment

It will be now demonstrated that $(\delta r_{RN}/a)_{min}$ of Eq. (13) is always smaller than the value that $(\delta r_{RN}/a)_{min}$ assumes when vectors $\boldsymbol{\delta e}$ and $\boldsymbol{\delta i}$ are parallel. From the vector norm properties

$$\|\boldsymbol{\delta e} + \boldsymbol{\delta i}\| \leq \|\boldsymbol{\delta e}\| + \|\boldsymbol{\delta i}\| \quad , \quad \|\boldsymbol{\delta e} - \boldsymbol{\delta i}\| \leq |\, \|\boldsymbol{\delta e}\| - \|\boldsymbol{\delta i}\| \,| \tag{14}$$

follows

$$\|\boldsymbol{\delta e} + \boldsymbol{\delta i}\| = \|\boldsymbol{\delta e}\| + \|\boldsymbol{\delta i}\| - c_1(\boldsymbol{\delta e}, \boldsymbol{\delta i}) \quad \text{with} \quad c_1 \geq 0 \quad \forall\, \boldsymbol{\delta e}, \boldsymbol{\delta i} \tag{15}$$

$$\|\boldsymbol{\delta e} - \boldsymbol{\delta i}\| = |\, \|\boldsymbol{\delta e}\| - \|\boldsymbol{\delta i}\| \,| + c_2(\boldsymbol{\delta e}, \boldsymbol{\delta i}) \quad \text{with} \quad c_2 \geq 0 \quad \forall\, \boldsymbol{\delta e}, \boldsymbol{\delta i} \tag{16}$$

From Equations (13), (15) and (16)

$$\left(\frac{\delta r_{RN}}{a}\right)_{min,\delta a=0} = \frac{\|\boldsymbol{\delta e}\| + \|\boldsymbol{\delta i}\| - |\, \|\boldsymbol{\delta e}\| - \|\boldsymbol{\delta i}\| \,| - (c_1 + c_2)}{2} \tag{17}$$

where $(\delta r_{RN}/a)_{min,\delta a=0}$ is the minimal value of $\delta r_{RN}/a$ when $\delta a = 0$. It follows

$$\left(\frac{\delta r_{RN}}{a}\right)_{min,\delta a=0} \leq \frac{\|\boldsymbol{\delta e}\| + \|\boldsymbol{\delta i}\| - |\, \|\boldsymbol{\delta e}\| - \|\boldsymbol{\delta i}\| \,|}{2} = \left(\frac{\delta r_{RN}}{a}\right)_{min,\delta a=0,\boldsymbol{\delta e}\|\boldsymbol{\delta i}} \tag{18}$$

$$\left(\frac{\delta r_{RN}}{a}\right)_{min} \leq \sqrt{\frac{\|\boldsymbol{\delta e}\| + \|\boldsymbol{\delta i}\| - |\, \|\boldsymbol{\delta e}\| - \|\boldsymbol{\delta i}\| \,|}{2} + \delta a^2 - 2\delta a \delta e} = \left(\frac{\delta r_{RN}}{a}\right)_{min,\boldsymbol{\delta e}\|\boldsymbol{\delta i}} \tag{19}$$

where $(\delta r_{RN}/a)_{min,\delta a=0,\boldsymbol{\delta e}\|\boldsymbol{\delta i}}$ is the minimal value of $\delta r_{RN}/a$ when $\delta a = 0$ and $\boldsymbol{\delta e}$ is parallel to $\boldsymbol{\delta i}$. Equations (18) and (19) show that the minimum collision risk is provided by parallel or anti-parallel relative e/i-vectors (i.e., $\varphi = \theta$) when $\delta a = 0$. If $\delta a \neq 0$ the additional condition to be added to that represented in Eq. (5) is that $\delta a \neq \delta e \cos(\theta - \varphi)$. In fact

looking for a condition on δa by which $\delta r_{RN}/a$ can assume a null value it can be written from Eq. (1)

$$\left(\frac{\delta r_{RN}}{a}\right)^2 = \delta a^2 - 2\delta a \delta e \cos(u-\varphi) + \delta e^2 \cos^2(u-\varphi) + \delta i^2 \sin^2(u-\theta) = 0 \tag{20}$$

$$\delta a = \frac{2\delta e \cos(u-\varphi) \pm \sqrt{-4\delta i^2 \sin^2(u-\theta)}}{2} \tag{21}$$

From Equations (20) and (21) results that the only real value of δa for which $\delta r_{RN}/a = 0$ is

$$\delta a = \delta e \cos(\theta - \varphi) \tag{22}$$

It can be concluded that for parallel $\boldsymbol{\delta e}$ and $\boldsymbol{\delta i}$ it has to be $\delta a \neq \delta e$ and in case these two vectors are perpendicular $\delta a \neq 0$. This statement can be easily noted by considering the geometry represented in Fig. 1. It can also be stated that for parallel or anti-parallel relative e/i-vectors, if $|\delta a| < \|\delta e\|$, the minimum separation decreases with an increase of $|\delta a|$ and vice versa it increases with an increase of $|\delta a|$ if $|\delta a| > \|\delta e\|$. Equations (18) and (19) imply that the choice of $(\delta r_{RN}/a)_{min,\boldsymbol{\delta e}\|\boldsymbol{\delta i}}$ as a collision risk parameter valid in all the possible cases actually minimizes the collision risk. Maintaining that it has to be $\delta a \neq \delta e$, Equations (18) and (19) yield

$$\left(\frac{\delta r_{RN}}{a}\right)_{min,\boldsymbol{\delta e}\|\boldsymbol{\delta i}} = \delta i^2 + \delta a^2 - 2\delta a \delta e \quad \text{if} \quad \|\delta e\| > \|\delta i\| \tag{23}$$

$$\left(\frac{\delta r_{RN}}{a}\right)_{min,\boldsymbol{\delta e}\|\boldsymbol{\delta i}} = (\delta a - \delta e)^2 \quad \text{if} \quad \|\delta e\| \leq \|\delta i\| \tag{24}$$

But as $\delta i^2 + \delta a^2 - 2\delta a \delta e < (\delta a - \delta e)^2$ if $\|\delta e\| > \|\delta i\|$, it results that in general the greatest value that the separation perpendicular to the flight direction is given by

$$\left(\frac{\delta r_{RN}}{a}\right)_{MIN} = |\delta a - \delta e| \tag{25}$$

The most conservative collision risk assessment for the general case can then be based on Eq. (25).

2.3. Inclusion of Uncertainties

The evaluation of the collision risk using Eq. (25) is of course conservative in all cases except when $\boldsymbol{\delta e}$ and $\boldsymbol{\delta i}$ are parallel and $\|\delta e\| \leq \|\delta i\|$, but it represents a single criteria valid in general and whose standard deviation can be easily evaluated as

$$var(|\delta a - \delta e|) = var(\delta a) + var(\delta e) - 2cov(\delta a, \delta e) \tag{26}$$

$$cov(\delta a, \delta e) = E(\delta a, \delta e) - E(\delta a)E(\delta e) \tag{27}$$

where var is the variance, cov is the covariance and E is the expected value.

The variance $var(|\delta a - \delta e|)$ and the standard deviation $\sigma(|\delta a - \delta e|)$ can be evaluated using the computational formula

$$var(|\delta a - \delta e|) = E\left((\delta a - \delta e)^2\right) - E^2(\delta a - \delta e) \tag{28}$$

$$\sigma(|\delta a - \delta e|) = \sqrt{var(|\delta a - \delta e|)} \tag{29}$$

3. Absolute and Relative Formation Control Algorithms

In this section the absolute and relative control algorithms which are combined, will be described. Analytical and numerical control methods have been considered. The absolute control methods considered are the closed-form analytical algorithm tested in flight with the Autonomous Orbit Keeping (AOK) experiment [4,5] on the PRISMA mission and a linear regulator [14]. The algorithm used for the Spaceborne Autonomous Formation-Flying Experiment (SAFE) [7] on the PRISMA mission, has been considered for the formation control.

3.1. AOK Closed-Form Analytical Control

In this case only the phase difference computed at the ascending node (AN) is controlled by means of along-track velocity increments. The phase difference δL_λ, measured along a parallel of latitude, is the longitude difference between the actual ground track and the track pertaining to a reference orbit. If da/dt and di/dt are taken as constants and di/dt can be taken as negligible compared to da/dt, δL_λ is found to have a near parabolic variation with time [4], as its second derivative is constant, and a simple control cycle can be imposed [15]. When δL_λ exceeds a pre-defined upper bound $\delta L_{\lambda_{MAX}}$ a corrective velocity impulse in the along-track direction of the spacecraft's orbit is applied as much as twice as would be necessary in order to return to the initial semi-major axis' value. As a result, just after the impulse the spacecraft's δL_λ begins to move towards the lower bound of the allowable band and when it has reached it, it drifts back to the upper limit where the next correction maneuver is made. The theoretical maneuver cycle T and the semi-major axis increments Δa to be applied are

$$\Delta a = 4\sqrt{\frac{T_E}{3\pi}\left(\frac{a}{R_E}\right)\left|\frac{da}{dt}\right|\delta L_{\lambda_{MAX}}} \qquad T = 4\sqrt{\frac{T_E}{3\pi}\left(\frac{a}{R_E}\right)\left|\frac{da}{dt}\right|^{-1}\delta L_{\lambda_{MAX}}} \tag{30}$$

where $T_E = 86400s$ is the mean period of the solar day. From the Gauss equations adapted for circular orbits [15], the velocity increment to be applied is

$$\Delta v_T = \left(\frac{\Delta a}{2a}\right) v \tag{31}$$

3.2. Linear Regulator for Absolute Orbit Control

The linear regulator is designed to control the system output $\mathbf{y} = (\delta L_\lambda, d(\delta L_\lambda)/dt)^T$, computed at the ascending node, by means of along-track velocity increments Δv_T. The linear

model used has state-space representation form

$$\dot{\boldsymbol{\epsilon}} = \mathbf{A}\boldsymbol{\epsilon} + \mathbf{B}\Delta\mathbf{v} \quad , \quad \mathbf{y} = \mathbf{C}\boldsymbol{\epsilon} \quad , \quad \boldsymbol{\epsilon} = a_{\mathcal{R}} \begin{pmatrix} \delta a & \delta i_y & \delta u \end{pmatrix}^T \quad , \quad \mathbf{B} = \begin{pmatrix} 2/n & 0 & 0 \end{pmatrix}^T \tag{32}$$

$$\mathbf{A} = a_{\mathcal{R}} \begin{pmatrix} & -\dfrac{AC_D\rho}{2ma_{\mathcal{R}}^2}\sqrt{\dfrac{\mu}{a}} & & 0 & 0 \\ \dfrac{21}{8}\left(\dfrac{R_E}{a}\right)^2 \dfrac{nJ_2}{a(1-e^2)^2}(5\cos^2 i - 1)e_y + \dfrac{AC_D\rho}{2m}n(e_x + \cos u) & & & 0 & 0 \\ -\dfrac{21}{8}\left(\dfrac{R_E}{a}\right)^2 \dfrac{nJ_2}{a(1-e^2)^2}(5\cos^2 i - 1)e_x + \dfrac{AC_D\rho}{2m}n(e_y + \sin u) & & & 0 & 0 \end{pmatrix} \tag{33}$$

$$\mathbf{C} = a_{\mathcal{R}} \begin{pmatrix} 0 & \dfrac{1}{\sin i_{\mathcal{R}}} & \dfrac{|\omega_E - \dot{\Omega}_{\mathcal{R}}|}{n} \\ \dfrac{A_{21}}{\sin i_{\mathcal{R}}} + \dfrac{A_{31}|\omega_E - \dot{\Omega}_{\mathcal{R}}|}{n} & 0 & 0 \end{pmatrix} \tag{34}$$

where a, e_x, e_y, i, Ω and u are the actual orbital elements, δa, δi_y, and δu are differences between actual and reference orbital elements, $a_{\mathcal{R}}$ and is the reference orbit's semi-major axis, R_E is the Earth's radius, J_2 is the geopotential second-order zonal coefficient, $n = \sqrt{\mu/a^3}$ is the mean motion, A is the spacecraft reference area, C_D is the drag coefficient, ρ is the atmospheric density, m is the spacecraft mass, ω_E is the Earth rotation rate and $\dot{\Omega}_{\mathcal{R}}$ is secular rotation of the reference line of nodes. The control input is

$$\Delta v_T = -\mathbf{G}\mathbf{y} = -(g_2 C_{21}\delta a + g_1 C_{12}\delta i_y + g_1 C_{13}\delta u)a_{\mathcal{R}} \tag{35}$$

where $\mathbf{G} = (g_1 g_2)$ is the gains matrix. The gain values chosen as a first guess are $g_1 = \text{sgn}(c_{21})\Delta v_{T_{\delta L}}/(a_{\mathcal{R}}\delta L_{\lambda_{MAX}})$ and $g_2 = \text{sgn}(c_{21})\Delta v_{T_{d\delta L}}/(a_{\mathcal{R}} d(\delta L_\lambda)/dt)_{MAX}$ where $\Delta v_{T_{\delta L}}$, $\Delta v_{T_{d\delta L}}$, $a_{\mathcal{R}}\delta L_{\lambda_{MAX}}$, $(a_{\mathcal{R}} d(\delta L_\lambda)/dt)_{MAX} \in \mathbb{R}^+$ are limits imposed by design and $\text{sgn}(c_{21})$ is the sign of c_{21}. The eccentricity vector can be passively controlled with a proper in-orbit location [1] of the along-track maneuver

$$u_M = \arctan\left(\frac{\delta e_y}{\delta e_x}\right) + k\pi \tag{36}$$

$$k = 0 \quad \text{if} \quad (\delta e_x \Delta v_T) < 0 \quad , \quad k = 1 \quad \text{if} \quad (\delta e_x \Delta v_T) > 0 \tag{37}$$

3.3. SAFE Closed-Form Analytical Control

Depending on the required orbit control accuracy, along-track, radial and cross-track maneuvers (in the form of single or double pulses) are executed at regular time intervals in a deterministic fashion according to the following solutions [6,7].
An arbitrary correction of the relative inclination vector $\boldsymbol{\delta i}$ can be realized through a single cross-track maneuver of size Δv_N at location u_m, given by

$$\Delta v_N na\|\boldsymbol{\delta i}_{aft} - \boldsymbol{\delta i}_{bef}\| = na\|\Delta\boldsymbol{\delta i}\| \quad \text{at} \quad u_m = \arctan(\Delta\delta i_y/\Delta\delta i_x) \tag{38}$$

where the superscripts aft and bef denote relative orbital elements immediately before

and after the maneuver under consideration. Eq. (38) represents the minimum delta-v solution for out-of-plane control.
The minimum delta-v solution for in-plane control provides an arbitrary correction of the remaining relative orbital elements according to the following double-impulse scheme

$$\Delta v_{T_1} = na(\Delta\delta a + \|\Delta\boldsymbol{\delta e}\|)/4 \quad \text{at} \quad u_{m_1} = \arctan(\Delta\delta e_y/\Delta\delta e_x) \tag{39}$$
$$\Delta v_{T_2} = na\Delta\delta a/2 \quad \text{at} \quad u_{m_2} = u_{m_1} + \pi \tag{40}$$

where along-track maneuvers in flight or anti-flight direction are separated by a half-orbit (the subscripts 1 and 2 indicate the first and second maneuvers of the same pair). Here, $\Delta\delta a$ and $\Delta\boldsymbol{\delta e}$ represent the desired corrections computed before the execution of the each individual maneuver of the pair.
An alternative approach for in-plane control is based on the execution of radial maneuvers separated by a half-orbit given by

$$\Delta v_{R_1} = na(\Delta\delta\lambda + \|\Delta\boldsymbol{\delta e}\|)/2\ ,\ \Delta v_{T_1} = na(\Delta\delta a/4) \quad \text{at} \quad u_{m_1} = \arctan(\Delta\delta e_y/\Delta\delta e_x) \tag{41}$$
$$\Delta v_{R_2} = -na\Delta\delta\lambda/2 \quad , \quad \Delta v_{T_2} = na\Delta\delta a/2 \quad \text{at} \quad u_{m_2} = u_{m_1} + \pi \tag{42}$$

The choice of the most appropriate in-plane control strategy, i.e. the usage of Eq. (39) or Eq. (41) is mission and application dependant. Pairs of tangential-only maneuvers ensure minimum propellant consumption, but when used for routine formation-keeping, cause unintentional drifts in along-track direction due to the continuous corrections of the semi-major axis. Pairs of radial maneuvers do not affect the semi-major axis and can realize smaller corrections of the relative orbital elements, due to the double delta-v consumption and the consequent longer burn times. The autonomous formation control (AFC) software module used during the SAFE experiment on PRISMA features two modes: the closed-loop along-track mode (CL-T) based on Eq. (39) and the closed-loop radial mode (CL-R) based on Eq. (41). CL-T is mainly used for large reconfigurations in along-track directions in rendezvous scenarios, whereas CL-R is preferred to accurately control the formation for tight reconfigurations at short separations in fly-around and inspection phases.

4. Numerical Simulations

The mission parameters of the TerraSAR-X/TanDEM-X formation are used for the numerical simulations in which one spacecraft keeps its absolute orbit's parameters within the control windows imposed around nominal values which characterize a reference orbit and the other controls instead the relative motion. The two spacecraft are assumed identical and the formation keeping is finalized to keep the spacecraft baseline in a defined control window and to keep a formation geometry safe from a collision risk (Sec. (2)). In this scenario the relative orbit control algorithm, besides commanding maneuvers for the formation maintenance, will also have to react to the absolute orbit's adjustments commanded on the other spacecraft by on-board autonomous absolute control system. A distributed control tasks assignment over time is suggested in order to keep the mass of the two spacecraft as similar as possible. With this approach the differential drag, and thus the fuel consumption, can be minimized and the mission lifetime maximized. The

Table 1. Propagation parameters

Spacecraft Physical Property	**TSX and TDX**
Mass [kg]	1341.17
Drag area [m^2]	3.2
Drag coefficient [-]	3.0
SRP effective area [-]	3.2
SRP coefficient [-]	3.0
Orbit Propagation	**Model**
Earth gravity field	GRACE GGM01S 70x70
Atmospheric density	Harris-Priester
Sun and Moon ephemerides	Analytical formulas [16]
Solid Earth, polar and ocean tides	IERS
Relativity effects	First order effects
Numerical integration method	Dormand-Prince
RO Propagation	**Model**
Earth gravity field	GRACE GGM01S nxn

important operational issue of optimal strategies for the tasks distribution is here not considered. The attention is instead focused on the performance and functional issues which arise when two different control algorithms work in parallel. Table 1 collects the spacecraft physical properties and force models used for the propagation of the simulated real and reference trajectories. In the simulations, run over 30 days, the absolute orbit of spacecraft TSX is controlled by the AOK analytical controller (Sec. (3.1)) or an in-plane linear regulator (Sec. 3.2). These absolute orbit control methods are combined with the autonomous relative analytical controller SAFE (Sec. (3.3)). The initial state of Table 2 has been used for TSX. The relative initial state of TDX is $(\delta a, a\delta e_x, a\delta e_y, a\delta i_x, a\delta i_y, a\delta u) = (0, 0, 300, 0, -400, 0)$ m in compliance with the collision risk minimization criteria of parallel or anti-parallel eccentricity and inclination vectors. The goal of the relative control is to keep this initial safe formation geometry. No navigation or actuator errors are included in the numerical simulations.

Table 2. TSX ECI Initial state and mean orbital elements

ECI state	$\mathbf{r_R}[\mathbf{m}]$	$\mathbf{r_T}[\mathbf{m}]$	$\mathbf{r_N}[\mathbf{m}]$	$\mathbf{v_R}[\mathbf{m/s}]$	$\mathbf{v_T}[\mathbf{m/s}]$	$\mathbf{v_N}[\mathbf{m/s}]$
	4888898.1	289059.5	-4852522.6	-5165.1	-1691.6	-5309.0
Mean orb. el.	$\mathbf{a}[\mathbf{m}]$	$\mathbf{e_x}[-]$	$\mathbf{e_y}[-]$	$\mathbf{i}[\mathbf{deg}]$	$\mathbf{\Omega}[\mathbf{deg}]$	$\mathbf{u}[\mathbf{deg}]$
	6883553.00	0.000026	0.001251	97.43	190.82	225.11

4.1. Combination of AOK, Linear and SAFE Controllers

4.1.1. AOK and Linear Absolute Orbit Control

Figures 2 and 3 show the ROE, the phase $a\delta L_\lambda$ and altitude $a\delta h = a(\delta a - \delta e_x)$ differences (computed at the ascending node), and the along-track control maneuvers Δv_T

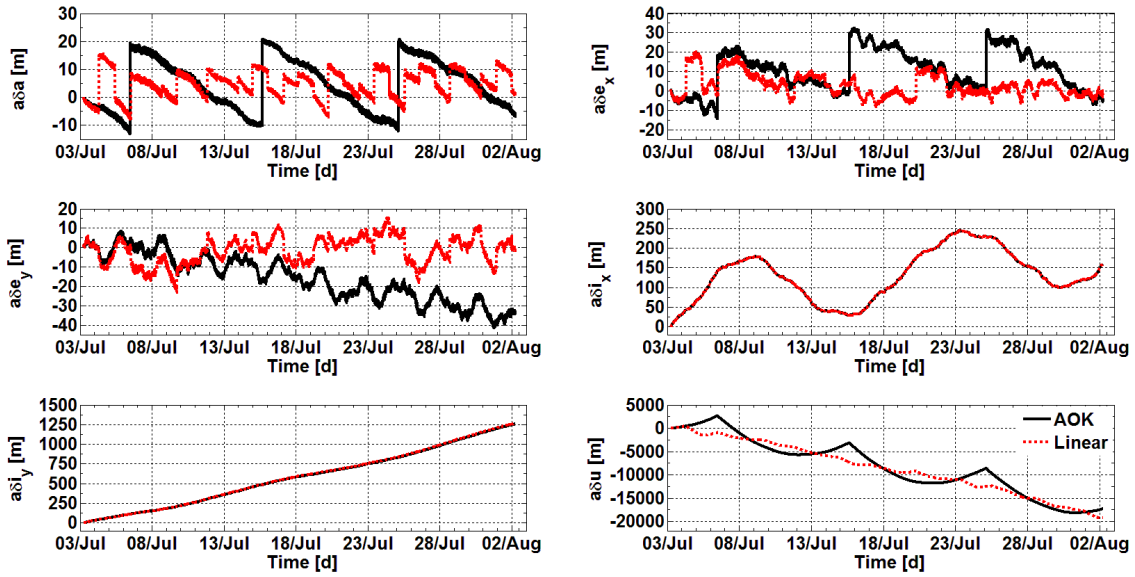

Figure 2. Relative orbital elements (Actual-RO)

executed by spacecraft TSX in case the absolute orbit is controlled by the AOK and linear controllers. The control window for AOK is $\delta L_{\lambda_{MAX}} = \pm 250$ m. The maneuver duty cycle is 24 hours and the parameters for the calculation of the linear regulator gains (Eq. (35)) are $a\delta L_{\lambda_{MAX}} = 30$, $a(\delta L_\lambda/dt)_{MAX} = 30/(86400)$, $(\Delta v_{T_{MAX}})_{\delta L} = 0.004$ and $(\Delta v_{T_{MAX}})_{\delta L/dt} = 0.001$. Table 3 collects the control performance and the maneuvers budget. Fig. 3 shows that AOK's control of δL_λ is characterized by a strict determinism. Three along-track maneuvers of about 0.17 m/s are executed with a maneuver cycle of about 10 days days. The vertices of the parabolas which characterize the time evolution of δL_λ are not placed in proximity of the lower bound of the control window at -250 m. This is due to the fact that the long term prediction of $\delta i_y/\sin i_{\mathcal{R}} + (|\omega_E - \dot{\Omega}_{\mathcal{R}}|/n)(\delta u - 2\delta e_y)$ [14] on which the maneuvers' computation is based, does not include the contribution of δi_x to the variation of δi_y but only that of δa. Indeed the weight of the contribution of δi_x to the variation of δL_λ increases with the duration of the maneuver cycle. Table 3 collects the control performance and the maneuvers budget. The total Δv spent by the AOK controller is 0.05 m/s. These simulation results can be compared with the flight data as well. The simulation foresees orbital maneuvers of about 0.017 m/s with a maneuver cycle of about 10 days whereas the flight data shows a mean maneuvers' value of 0.015 m/s with a mean maneuver cycle of about 8 days. Though these first results state that the AOK controller has a similar cost performance with respect to the orbit control system of TSX [1] a more accurate statistical analysis has to be carried on.

As shown by Fig. 3 the placement of the maneuvers with the rule of Eq. (36), allows the control of the eccentricity vector (and thus $a\delta h$) by the linear regulator whereas the analytical controller has no eccentricity vector control capability as it executes the maneuvers only at the orbit's ascending node. The linear regulator has a control accuracy better than the analytical controller but at a double cost of 0.12 m/s as can be seen in Table 3.

The main difference between the AOK analytical controller and the numerical regulators

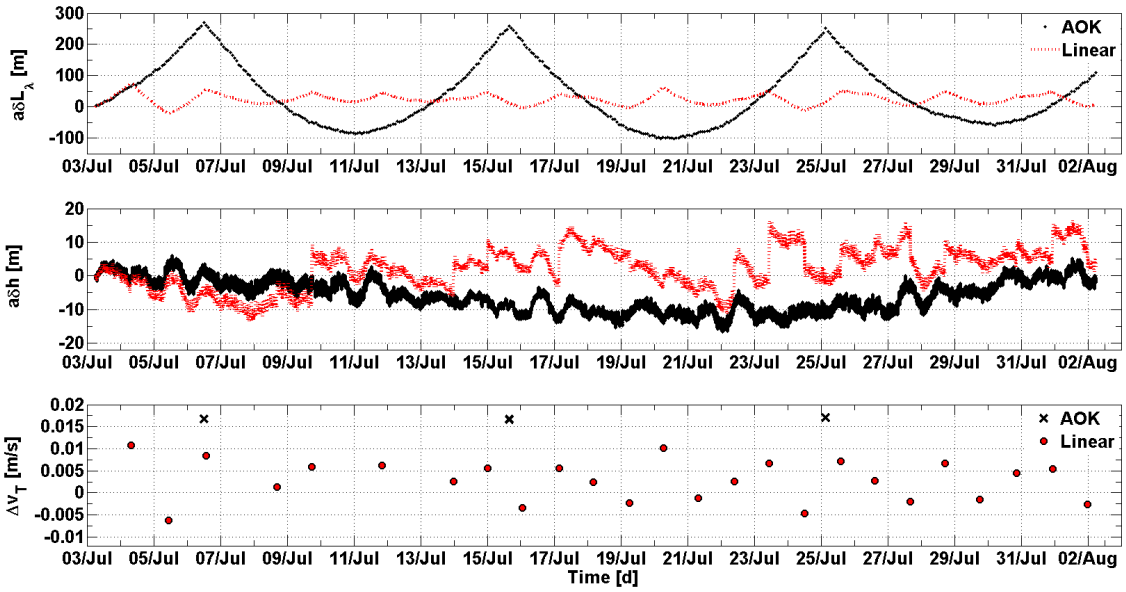

Figure 3. Phase and altitude differences at the AN and executed orbital maneuvers

is that the AOK's maneuvers computation is based on a long term prediction of δa highly dependent on the correct estimation of the semi-major axis decay rate da/dt. On the other hand, the linear regulator computes the orbital maneuvers with a pure feedback logic based on the values of the control gains. This fundamental difference between the two control strategies is demonstrated by examining the orbital maneuvers in Fig. 3. The linear regulator commands a maneuver at each duty cycle whereas the AOK control system commands larger maneuvers at a deterministic maneuvers cycle of about 10 days. The AOK algorithm has an optimal control performance in terms of Δv budget.

Table 3. Control performance and maneuvers budget of AOK control

AOK	**Min**	**Max**	**Mean**	σ	**RMS**	**AOK**	**Min**	**Max**	**TOT**
$a\delta L_\lambda$ [m]	-101.97	269.71	40.87	100.31	108.31	Δv_T [m/s]	0.01663	0.01703	0.0504
$a\delta h$ [m]	-16.63	6.11	-6.15	4.65	7.71				
Linear	**Min**	**Max**	**Mean**	σ	**RMS**	**Linear**	**Min**	**Max**	**TOT**
$a\delta L_\lambda$ [m]	-22.6	76.44	23.42	16.07	28.41	Δv_T [m/s]	-0.0062	0.0108	0.1189
$a\delta h$ [m]	-13.33	16.59	1.85	6.07	6.34				

4.1.2. SAFE Formation Control

Figures 4, 5 and 6 show the ROE, the phase $a\delta L_\lambda$ and altitude $a\delta h = \delta a - \delta e_x$ differences (computed at the AN), the baseline and the orbital maneuvers of TDX with respect to TSX when the relative orbit of the TDX spacecraft is controlled by the SAFE controller and the absolute orbit of TSX is controlled by the AOK or linear controller (Sec. (4.1.1)).

The on-ground baseline is computed as $a\delta L = \sqrt{a\delta L_\lambda^2 + a\delta L_\varphi^2}$ where $a\delta L_\varphi$ is the normalized difference of TSX and TDX latitudes when TSX passes at the AN. The control

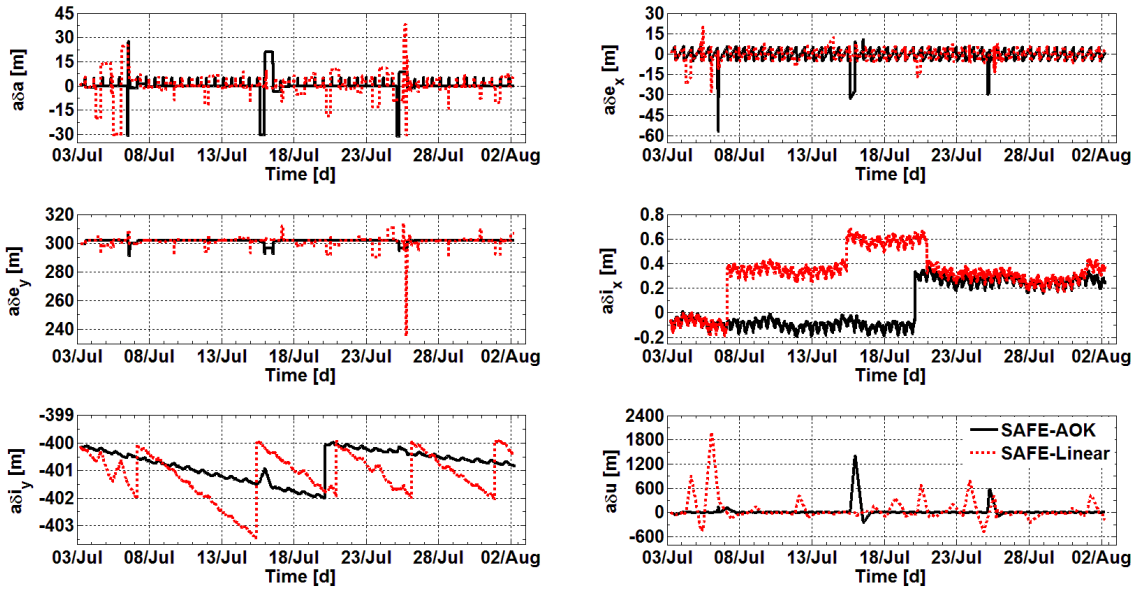

Figure 4. Relative orbital elements

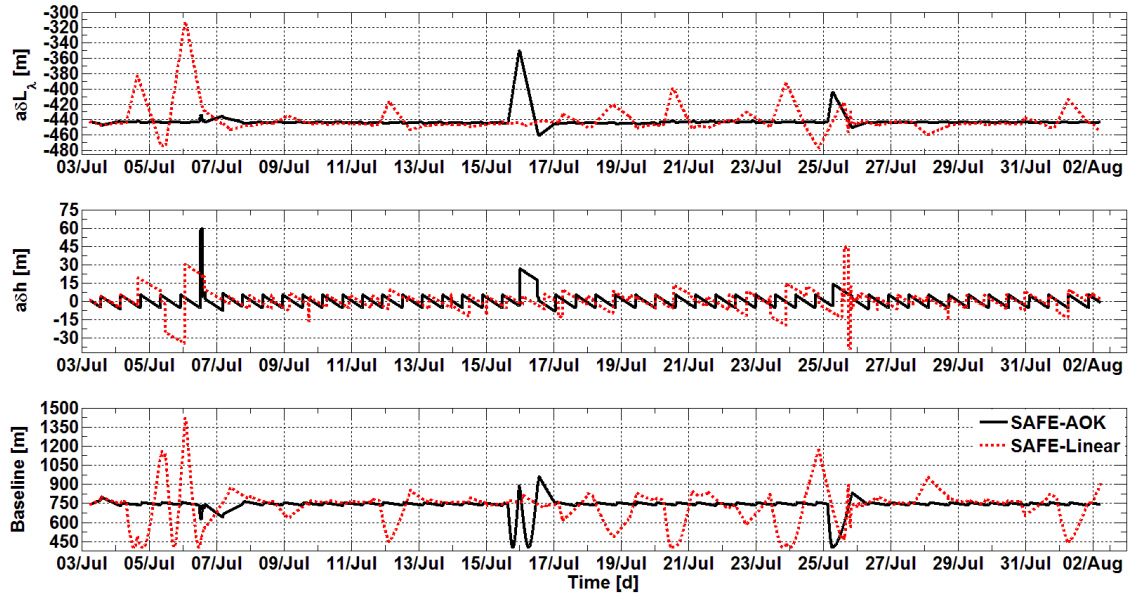

Figure 5. Phase and altitude differences and baseline at the AN

windows of $a\delta e$ and $a\delta i$ are respectively 5 m and 2 m.

If the absolute orbit of TSX is controlled by AOK, the formation control is characterized by a strict determinism with an in-plane maneuver cycle of 6 hours during the steady-state phases as can be observed in Fig. 6. Only one out-of-plane maneuver of 0.002 m/s is executed when $a\delta i_y$ exceeds the maximum allowed deviation of 2 m. The SAFE controller reacts to the absolute orbit control maneuvers of TSX which causes a sudden

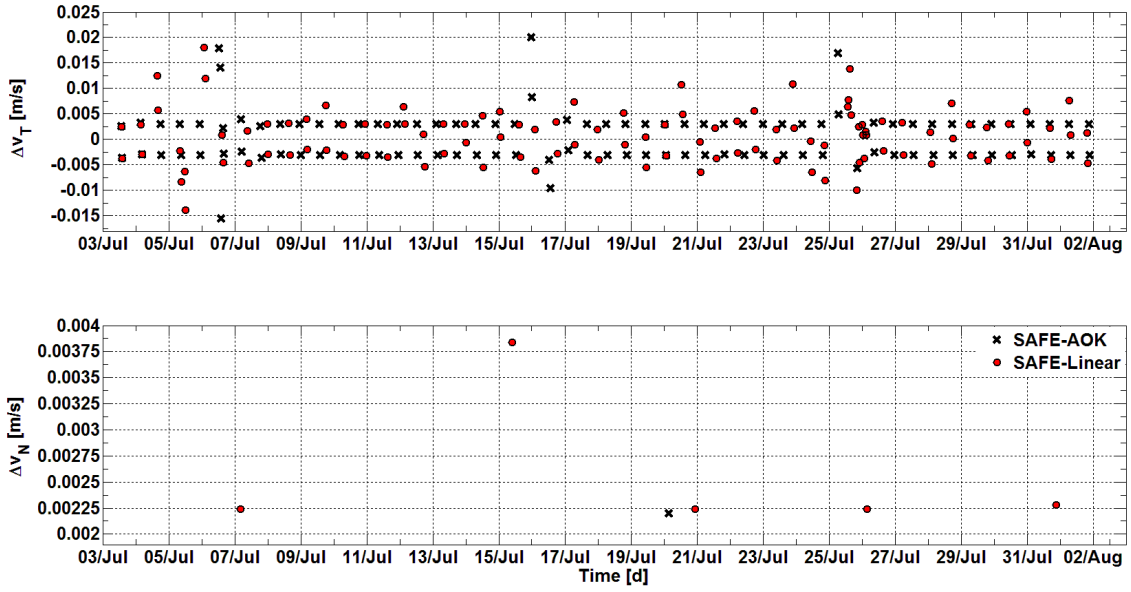

Figure 6. Executed formation control maneuvers

change of δa, δe_x and δe_y and re-acquires the formation configuration in about 1.5 days. Table 4 collects the statistical quantities of the values assumed by $a\delta L_\lambda$ and $a\delta h$ during the steady-state phase between the 7th and 15th of July. The quantity δL_{err} indicates the difference between the actual and the nominal values of the on-ground baseline. The control accuracies of $a\delta L_\lambda$ and $a\delta h$ in the steady-state phase are respectively 1.5 and 6 m. The total Δv spent for the formation keeping during the simulation time of one month is 0.4 m/s. The baseline, controlled with an accuracy of 7 m (1 σ) has a nominal value of 742 m and reaches a minimum and maximum length of respectively 400 and 950 m during the formation re-acquisition phases. This simulation foresees formation keeping in-plane maneuvers for an amount of 0.008 m/s every 14 hours (0.04 every 3 days) whereas the flight data of TDX show a mean in-plane maneuvers' value of about 0.02 m/s every 3 days. The foreseen out-of-plane maneuvers budget of about 0.005 m/s once per month is very similar to what can be read from the flight data. As for the absolute control, these results has to be treated cautiously as well and deserve a deeper analysis.
If the absolute orbit of TSX is controlled by the linear regulator, the lack of determinism in

Table 4. Control performance and maneuvers budget of AFC relative control

SAFE-AOK	**Min**	**Max**	**Mean**	σ	**RMS**	**SAFE-AOK**	**Min**	**Max**	**TOT**
$a\delta L_\lambda$ [m]	-445.35	-442.99	-444.14	0.51	444.14	Δv_T [m/s]	-0.0155	0.0201	0.3997
$a\delta h$ [m]	-8.44	59.55	0.58	5.21	5.25				
$a\delta L_{err}$ [m]	-9.1	16.15	3.71	6.01	7.06	Δv_N [m/s]	0	0.0022	0.0022
SAFE-Lin.	**Min**	**Max**	**Mean**	σ	**RMS**	**SAFE-Lin.**	**Min**	**Max**	**TOT**
$a\delta L_\lambda$ [m]	-477.38	-312.3	-439.62	18.39	440.0	Δv_T [m/s]	-0.0377	0.0269	0.5166
$a\delta h$ [m]	-38.64	44.94	0.4	8.42	8.43				
$a\delta L_{err}$ [m]	-338.72	676.17	-12.56	133.9	134.48	Δv_N [m/s]	0	0.0038	0.0128

the absolute orbit control is reflected by the relative control as can be observed comparing the absolute and relative orbit maneuvers displayed in Figures 3 and 6. The SAFE control system has to react to the orbital maneuver commanded by the linear regulator on-board TSX once per day. The control accuracies of $a\delta L_\lambda$ and $a\delta L_h$, displayed in Table 4, are respectively 21 and 10 m. The baseline is controlled with an accuracy of 134 m (1 σ) and reaches a minimum and maximum length of respectively 400 and 1400 m. The total Δv spent is 0.53 m/s.

5. Conclusions

The combination of autonomous absolute and relative control of a two spacecraft formation in low Earth orbit has been studied by means of numerical simulations. One of the two spacecraft controls its absolute orbit while the other keeps the formation geometry. A closed-form analytical method and a linear regulator has been considered for the absolute orbit control. Both this controllers have been combined with a formation keeping system, based on the closed solutions of an analytical algorithm. The most cost effective solution fulfilling the control accuracy requirements is the combination of the analytical controllers. Differently from the linear regulator, the absolute orbit analytical controller executes larger maneuver with a deterministic and longer control cycle. Since the formation keeping system of one spacecraft has to react to each absolute orbit control maneuver of the other spacecraft and reacquire the safe formation geometry, a longer absolute control cycle results in a more cost effective formation control. Comparing the simulation results with actual mission data, it results that, in terms of maneuvers budget, the on-board is more expensive than the ground-based combined control.

References

[1] D'Amico, S., Kirschner, M., and Arbinger, C.,"Precise Orbit Control of LEO Repeat Observation Satellites with Ground-in-the-Loop", Tech. Rep. DLR-GSOC TN 04-05, Deutsches Zentrum für Luft und Raumfahrt, Oberpfaffenhofen, Germany, 2004.

[2] Montenbruck, O., Kahle, R., D'Amico, S., and Ardaens, J.-S."Navigation and Control of the TanDEM-X Formation", *The Journal of the Astronautical Sciences*, Vol. 56, No. 3, Jul.-Sept. 2008, pp. 341-357.

[3] Lamy, A., Julien, E., and Flamenbaum, D.,"Four Year Experience of Operational Implementation of Autonomous Orbit Control: Lessons Learned, Feedback and Perspectives", Proceedings of the *21st International Symposium on Space Flight Dynamics*, 2009, Toulouse, France.

[4] De Florio, S., and D'Amico, S.,"The Precise Autonomous Orbit Keeping Experiment on the Prisma Mission", *The Journal of the Astronautical Sciences*, Vol. 56, No. 4, Oct.-Dec. 2008, pp. 477-494.

[5] De Florio, S., D'Amico, S., and Radice, G.,"Flight Results of the Precise Autonomous Orbit Keeping Experiment on the Prisma Mission", *AIAA Journal of Spacecraft and Rockets*, doi:10.2514/1.A32347.

[6] D'Amico, S.,"Autonomous Formation Flying in Low Earth Orbit", PhD thesis, Technische Universiteit Delft, 2010. ISBN 978-90-5335-253-3.

[7] D'Amico, S., Ardaens, J.-S., and Larsson, R.,"Spaceborne Autonomous Formation Flying Experiment on the PRISMA Mission", *AIAA Journal of Guidance, Navigation and Control*, vol.35, no.3, pp 834-850, 2012, doi:10.2514/1.55638.

[8] Ardaens, J.-S., and D'Amico, S.,"Spaceborne Autonomous Relative Control System for Dual Satellite Formations", *AIAA Journal of Guidance, Navigation and Control*, Vol. 32, No. 6, pp. 1859-1870, Nov.-Dec. 2009, doi:10.2514/1.42855.

[9] Ardaens, J.-S., and Fischer, D.,"TanDEM-X Autonomous Formation Flying System: Flight Results", *Journal of Mechanics Engineering and Automation*, Vol. 2, No. 5, pp. 332-339, May 2012, ISSN 2159-5283 (online).

[10] Kahle, R., Schlepp, B., and Kirschner, M.,"TerraSAR-X/TanDEM-X Formation Control - First Results from Commissioning and Routine Operations", *Journal of Aerospace Engineering, Sciences and Applications*, Vol. 3, No. 2, pp. 16-27, May-Aug. 2011, ISSN:2236-577X.

[11] Eckstein M.C., Rajasingh C.K., and Blumer P.,"Colocation strategy and collision avoidance for the geostationary satellites at 19 degrees west", Proceedings of the *CNES International Symposium on Space Flight Dynamics*, 6-10 Nov., 1989, Toulouse, France.

[12] Montenbruck, O., Kirschner, M., D'Amico, S., and Bettadpur, S.,"E/I-vector separation for safe switching of the GRACE formation", *Journal of Aerospace Science and Technology*, Vol. 10, No. 7, pp. 628-635, 2006, doi:10.1016/j.ast.2006.04.001.

[13] Bodin, P., Noteborn, R., Larsson, R., Karlsson, T., D'Amico, S., Ardaens, J.-S., Delpech, M., and Berges, J.-C.,"The Prisma Formation Flying Demonstrator: Overview and Conclusions from the Nominal Mission", Proceedings of the *35th Annual AAS Guidance And Control Conference*, AAS 12-072, 3-8 Feb. 2012, Breckenridge, CO, USA, ISBN 978-0-87703-585-5.

[14] De Florio, S., D'Amico, S., and Radice, G.,"Precise Autonomous Orbit Control in Low Earth Orbit", Proceedings of the *AIAA/AAS Astrodynamics Specialist Conference and Exhibit*, 13-16 Aug. 2012, Minneapolis, MN, doi:10.2514/6.2012-4811.

[15] Micheau, P.,"Spaceflight Dynamics, Vol. I, Chap. Orbit Control Techniques for LEO Satellites", Toulouse, France, Cepadues-Editions, 1995, ISBN:2-85428-376-7.

[16] Montenbruck, O., and Gill, E.,"Satellite Orbits - Model, Methods and Applications", Springer Verlag, Heidelberg, Germany, 2000, ISBN:3-540-67280-X.